





SIGNAL PROCESSING

ALGORITHMS, ARCHITECTURES, ARRANGEMENTS, AND APPLICATIONS

SPA 2023

September 20th - 22nd, 2023, Poznań, POLAND

Contour Extraction of Surgical Stoma Surfaces Using 2.5D Images from Smartphone 3D Scanning

Francisco Luquin Monroy
Electrical and Computer Engineering Department
University of Washington
Seattle, United States
luquif@uw.edu

THE INSTITUTE OF ELECTRICAL AND ELECTRONICS ENGINEERS INC

Electrical and Computer Engineering Department
University of Washington
Seattle, United States
rhussein@uw.edu

Rania Hussein

Abstract— In this paper, we present a technique for extracting stoma outlines from 2.5D images acquired through smartphonebased 3D scanning. Accurate stoma outlining plays a crucial role in tailoring ostomy wafers, thereby minimizing stoma damage, preserving the health of surrounding skin, and ultimately enhancing the health-related quality of life for stoma patients. Our proposed method leverages a widely used contour algorithm and incorporates error analysis to assess its effectiveness and precision. Through a series of experiments, we investigate the potential and limitations of smartphone 3D scanning in achieving precise and personalized stoma contouring. Additionally, we introduce an error metric to evaluate the performance of the technique quantitatively. Our findings shed light on the possibilities for advancements in 3D scanning technology and image processing techniques, marking a significant step towards harnessing smartphone technology for improved ostomy management and

Keywords-Stoma; image segmentation; Stoma outline extraction; 2.5D height gradient images; smartphone imaging

I. INTRODUCTION

Individuals who have undergone ostomy surgery have a surgical opening, or a stoma, created in their abdomen to facilitate the elimination of bodily waste. A customized adhesive silicon wafer is placed around the stoma to protect the surrounding skin and serve as an attachment point for an ostomy bag. The current method of preparing the wafer, often using circular paper templates, is time-consuming and inexact. However, stomas are seldom perfectly round, leading to potential inaccuracies in the resulting contour. A large cut can expose peristomal skin to fecal matter, resulting in potential skin erosion, infections, or leakage. Conversely, a small cut can inflict trauma to the stoma, possibly causing bleeding and stoma suffocation. Moreover, during the initial period following surgery, patients are most likely to make mistakes in managing their stomas. Therefore, the system depicted in Figure 1 is under development as a potential solution to assist stoma patients in obtaining customized wafers. An essential component of this system is the precise extraction of the stoma's contour [1, 2].

In the field of external medical imaging, the focus has been mainly on wound assessment, utilizing primarily 2D imaging techniques. The authors have previously highlighted the

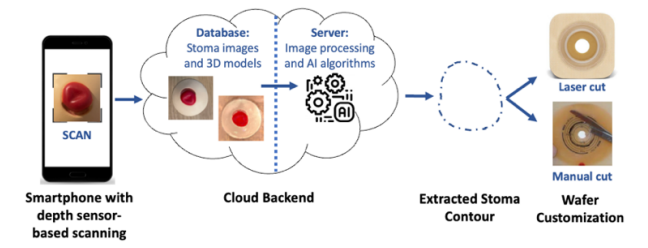


Fig. 1. The proposed architecture of the software-based ostomy management system, illustrating the flow of data from stoma scan and image acquisition to customized wafer cutting methods.

limitations of 2D imaging for ostomy management [1, 2]. The contours derived from 2D images are susceptible to distortion due to lighting, the angle of capture, and body curvature [3, 4]. Consequently, a trained user must capture images as perpendicularly as possible to the stoma while mitigating factors that could impact the image quality, such as body creases or nearby hernias, common in ostomates [5].

The requirements of 2D imaging place significant demands on potential users and raises questions about its practicality for untrained individuals. Hence, there is a pressing need for more reliable and user-friendly technology to facilitate convenient, athome care without compromising quality. Such a solution would have broad impacts, extending to similar fields in healthcare and telehealth, such as wound management, dermatology, and burn management.

Previous studies have explored wound measurement and analysis using both 2D images [6, 7] and 3D models, reconstructed from structured light [8], stereophotogrammetry [9-11], 3D laser scanners [12-15], and other imaging techniques [16-18]. Methods providing 3D-based measurements are particularly compelling due to their enhanced accuracy and robustness in capturing an object's geometry. However, the main limitation of these depth-scanning technologies lies in their complexity, cost, and consequent inaccessibility. With many modern smartphones now equipped with built-in laser scanning systems, opportunities arise for a more holistic ostomy wound management system.

Past studies have explored using the Intel RealSense D415 and D435 for stoma imaging [13]. While these methods provide valuable insight, the error tolerance is too large for our application and could harm the stoma. Furthermore, these approaches require a complex setup that is impractical for a home environment and needs manual camera adjustment, limiting its usefulness in at-home care [13].

Similarly, a study comparing the accuracy of eight scanning devices, including the Kinect V1 and V2 and the Structure Sensor, identified the Structure Sensor as the most suitable low-cost device for orthopedic reconstruction [19]. However, even this device, deemed the most accurate low-cost scanner, is inaccessible for most patients due to its high cost and requirement for an iPad.

The need for accurate, user-friendly, and cost-effective 3D imaging technology for stoma contouring is clear. Our previous work showed that the iPhone 12 Pro's scanning systems had an average error of less than 2 mm [1]. In this study, we further explore this technology's potential by scanning six stoma models with the iPhone and extracting the contours using Suzuki's rules-based contour algorithm, a contour detection method implemented in the OpenCV library and widely recognized by its use in image processing, on 2.5D images [20]. This process aims to determine whether the topological nature of stomas allows for simple and reliable extraction. Our findings indicate that rules-based algorithms may not be robust or stable enough for effective stoma management due to the complex geometry and color of the stoma and surrounding area.

In the following sections, we discuss our methodology for extracting stoma outlines, explore the potential and limitations of smartphone-based 3D scanning for stoma contouring, and analyze errors associated with Suzuki's contour algorithm [20]. This paper concludes with a discussion of the implications of our findings and avenues for future research.

II. METHODOLOGY

A. Data Collection

To accommodate the real-world diversity, our methodology involved using six distinct stoma models, as listed in Table 1, that demonstrate only some of the variance in color, size, and surrounding environment of stomas.

TABLE I. STOMA MODELS DESCRIPTION AND IMAGES

ID	Description	Image	Dimensions (Major Axis x Minor Axis x Height)
S1	Recessed stoma		24 mm x 18 mm x 2 mm

S2	Flush stoma		24 mm x 21 mm x 1 mm
S3	Mushroom stoma		27 mm x 27 mm x 21 mm
S4	Double barrel stoma	A LES	64 mm x 33 mm x 11 mm
S5	Ischemic stoma	N. C.	49 mm x 47 mm x 20 mm
S6	Loop stoma		47 mm x 28 mm x 16 mm

Typically, an ostomy wafer is cut to match the shape of the stoma with a one-fourth to one-eight-inch margin. However, in this study, we evaluate the original stoma contour to reduce the complexity of contour expansion. The shape of the stoma is ideally extracted as the contour of the stoma from an overhead perspective, and this is currently conducted subjectively. To extract an accurate ground truth contour for our study, we placed the models on a flat cardboard surface with a checkered pattern. The unique shape of the cardboard surface and the 1 cm checkered pattern spacing facilitated image alignment and scaling, respectively. The stoma models were photographed with an iPhone 12 Pro's back camera. To minimize perspective effects, the iPhone was secured on a platform, ensuring it was parallel, within 1 degree in the X and Y direction, with the surface on which the stoma model was placed, and the stoma models were placed roughly in line with the camera.

To extract the contour of the stoma with a system like the one depicted in Figure 1, we scanned the stomas with the iPhone 12 Pro using the iPhone application and scanning method described in our previous paper [1]. To accurately compare the extracted contour and the ground truth contour, the stoma was scanned after imaging to preserve its orientation on the cardboard surface. This process will produce colorless 3D models, as shown in Figures 2 (a) and (b). The resulting 3D models were processed using the CloudCompare software, scaled so that the model's units match to millimeters, cropped to contain the stoma and cardboard surface, leveled so the cardboard surface is the X-Y plane, and aligned to match the orientation of the cardboard in the ground truth images.

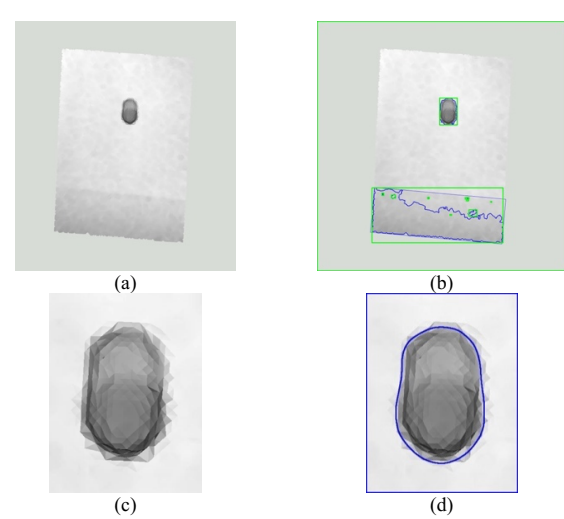


Fig. 2. The process of generating the contour. The 3D model is leveled, after which a height gradient is applied, resulting in the overhead screenshot depicted in (a). OpenCV's algorithm is employed to identify all possible contours, as illustrated in (b), each of which is subsequently scored using (1). The overhead image is then cropped to focus on the highest-scoring contour, as shown in (c). OpenCV's algorithm is reapplied to identify all contours within the cropped image, demonstrated in (d). The highest-scoring contour is then selected, which is the center contour around the stoma in (d).

B. Ground Truth Contour Extraction

The images were processed using Fiji, an open-source image processing program, to extract the ground truth contours. Prior to processing the images, the ground truth images were cropped and then finely aligned using rigid-body registration, specifically with the Scale-Invariant Feature Transform (SIFT) algorithm, a technique that identifies uses key features within a set of images to ensure accurate alignment, within Fiii. A rigidbody registration means only translations and rotations can be used, ensuring the final contour is not altered. Although not directly observable, this alignment occurred on the images in the 'Ground Truth Contours' column of Table II. Extracting the contours included several steps: color thresholding to highlight the stoma shape, conversion to a binary mask, removing background objects, filling in any holes in the binary mask, and overlaying the mask onto the original stoma image to correct any discrepancies manually. The ground truth contour was then obtained from the outer set of pixels of the mask. The error introduced from manual correction was less than a 0.15 mm deviation from the optimal contour at any point.

C. Contour Extraction

We aimed to simplify the complexity of processing 3D models by focusing on the topology of the stoma using 2.5D images with which we can apply 2D imaging techniques. In order to create 2.5D images from the 3D mesh, we applied a height gradient, which assigns a color to each height level, creating a visual representation of the height of the different parts of a 3D model. The colors assigned to the different heights form a gradient, which creates the perception of depth of a 3D model in a 2D image. In our case, we applied a grayscale gradient ranging from gray at the lowest points, white for the mid-range, and gray again for the highest points. This height

gradient was applied using the Python library vtkplotlib. Once the gradient was applied, an overhead screenshot of the model was captured to produce the 2.5D image. To extract a contour that can be compared, the scale of the 2.5D image was obtained by comparing the X-Y distance of two recognizable points on the 3D model to two points on the 2.5D image. The 2.5D images were then scaled down to match the scale of the ground truth images. Registration algorithms, such as SIFT and TurboReg on Fiji, were trialed for finely aligning the 2.5D images to the ground truth images but had limitations. Hence, we used visual alignment and looked to see that the cardboard surface, which had an asymmetrical shape with straight lines, was centered and had the same angle.

With 2.5D images, our method extracts the stoma contour with the process shown in Figure 2. From the 2.5D image, as shown in Figure 2 (a), OpenCV's contour algorithm is used to find all the contours from this image, depicted in Figure (b), from which to narrow down.

Equation (1) is used to score the different contours and select the contour representing the stoma. The score aims to quantify the largest contour containing the uniformly darkest set of pixels. A contour's score is inversely proportional to the mean intensity of the set of pixels it contains - a 2.5D image will highlight the stoma with darker pixels due to its typical height. The score should also be proportional to the area of the contour to account for cases where a smaller contour encircles a subset of pixels in the stoma. The last term increases the score of contours with a set of pixels with the smallest standard deviation. To avoid a division by zero in the cases where the mean or standard deviation is 0, an offset is added to both terms, and they are further rewarded by setting exponential variables l and k to be large numbers, which from experiments, we found an l and k of 80 and 3, respectively, worked well.

Score = area
$$\cdot \frac{1}{(\text{mean pixel intensity} + 0.1)^k} \cdot \frac{1}{(\text{std of pixel intensity} + 0.1)^l}$$
 (1)

Once the highest-scoring contour is selected, the image is cropped (Figure 2 (c)), and the contours are found and scored again to ensure a precise contour is extracted (Figure 2 (d)). Since the 3D models have quite a bit of tessellation where the stoma models meet with the background, blurring is applied to minimize the effects on the extracted contour.

D. Error Evaluation

To evaluate the contours, we conducted an error-based evaluation. The minimum distance to the ground truth contour is calculated for each point in the extracted contour. Our objective was to achieve an absolute error of less than 2 mm at every point, as deviations larger than this could potentially harm the stoma or expose surrounding skin to fecal matter.

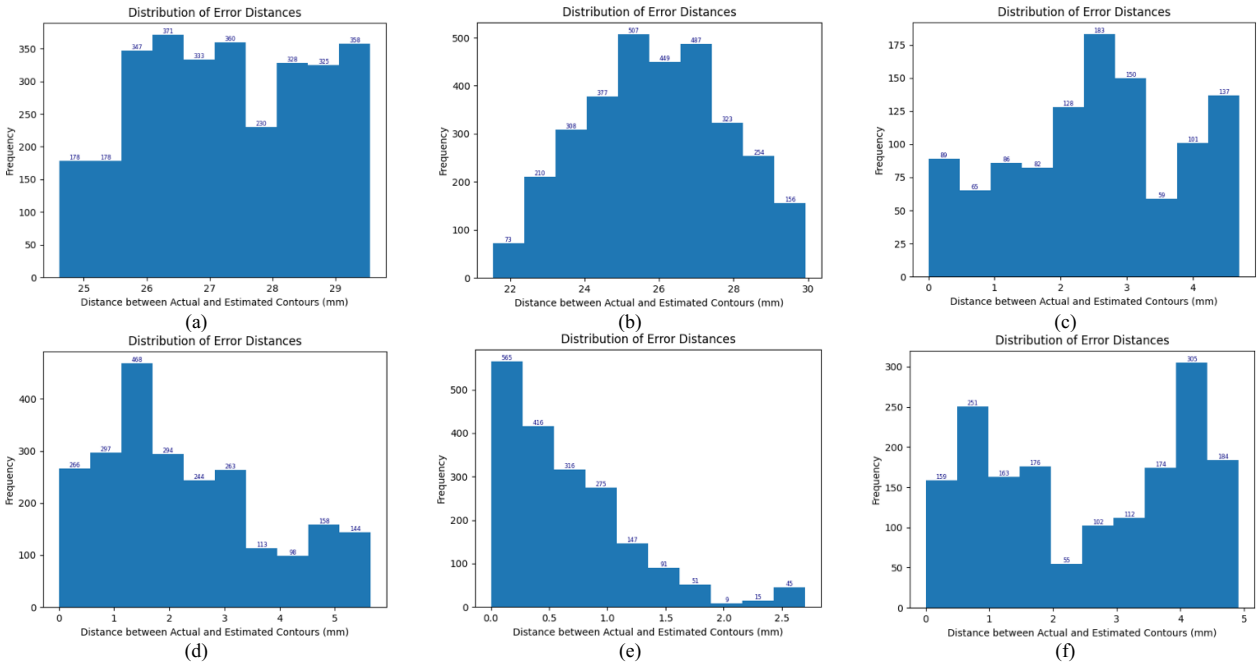


Fig. 3. Distribution of Error Distances between Actual and Estimated Stoma Contours. The histograms show the frequency (y-axis) of specific error distances (x-axis) for each stoma model: S1 (a), S2 (b), S3 (c), S4 (d), S5 (e), and S6 (f).

III. RESULTS

Our method for extracting contours from stoma images was tested on six different stoma models, yielding results that varied in terms of accuracy and consistency.

A. Contour Overlap

Table 2 presents the visual comparison of the ground truth contours, the extracted contours, and their overlaps for each stoma model. In the fourth column, the X-axis and Y-axis in each figure represent distance in millimeters. As can be observed, the extracted contours, depicted in red, align closely with the ground truth contours, shown in blue, for all but two of the stoma models. The overlapping areas, represented in purple, highlight the regions of agreement between the extracted and ground truth contours. Overall, our method achieved an average error of 10 mm, with the highest average error being 27.3 mm and the lowest average error being 0.67 mm.

B. Error Distribution

Figure 3 shows histograms of the absolute error distributions for each stoma model. The minimum Euclidean distance to the ground truth contour was calculated for each point in the extracted contour. The X-axis represents the distance error in millimeters, while the Y-axis indicates the frequency of each error magnitude.

The error distributions exhibit some variability across the different stoma models, with most errors falling within the range of 0 to 5.5 mm. Interestingly, stomas S1 and S2 demonstrated the highest frequency of errors within the range

of 21 to 30 mm, which we will discuss in detail in the discussion section.

IV. DISCUSSION

Our method achieved the best results with an average error of 0.67 mm on S5. However, S3, S4, and S6 exhibited greater error ranges of up to 5.65 mm. The main sources of these errors were the tessellation at the intersection between the stoma model surface and the background and the misalignment of contours.

Stomas S1 and S2 presented challenges due to their complex shapes and surroundings. The height variations and level positioning of S1's stoma and surrounding skin caused our method to contour the skin instead of the stoma. Similarly, S2's flush stoma, being level with the flat surrounding skin, also caused the algorithm to contour the skin rather than the stoma.

This complexity underscores why we opted for a 3D imaging approach over traditional 2D imaging. 2D imaging is often complicated by factors such as lighting, angle of capture, and training, making it unsuitable for patient self-care. Conversely, 3D imaging mitigates these issues, reducing the need for perfect imaging capture and lessening the importance of lighting due to the added geometric information.

Yet, the challenge with 3D imaging lies in the complexity of processing and developing algorithms. Considering the intricate nature of 3D models and the diverse topology of stomas, an artificial intelligence approach would demand an impractically large sample size. Therefore, we employed a rules-based approach using OpenCV's algorithm and relied on

the typical stoma topology to develop 2.5D images for the contour extraction algorithm.

However, the results were suboptimal. Although our approach showed promise with typical stomas that protrude from the skin, it faltered when faced with the complex environment surrounding the stoma. This, similarly, hints at the

issues we would face if scanning the stoma models on a mannequin.

Future research should focus on improving the accuracy of 3D models and incorporating color. This will facilitate alignment and reduce tessellation, addressing two of the main sources of error in our study. We also suggest further

TABLE II. COMPARISON OF GROUND TRUTH AND EXTRACTED CONTOUR FOR EACH STOMA MODEL

ID	Ground Truth Contour	Extracted Contour	Overlap of Ground Truth and Extracted Contour
S1			76.23 65.34 54.65 9 32.67 21.78 10.89 0.0 10.96 21.93 32.89 43.85 54.82 65.78 76.74 Distance (mm)
S2			66.7 - 55.58 - 65.58 -
S3			20.35 26.02 21.68 17.34 00 00 4.34 00 00 4.68 9.37 14.05 18.74 23.42 28.11 32.79 Distance (mm)
S4			71.65 61.41 51.18 10 10 10 10 10 10 10 10 10 10 10 10 10
S5			23.22 44.84 27.37 - UL 29.89 - 1 22.42 - 1 14.95 - 1 7.47 - 0 0 0 7.12 14.25 21.37 28.49 35.62 42.74 49.86 Distance from
S6			60.19 40.19 33.49 40.19 20.09 33.49 40.70 33.49 40.70

exploration into AI algorithms to identify and contour stomas within 3D scans.

V. CONCLUSION AND FUTURE WORK

In this paper we illustrated the potential of smartphones in scanning stomas to generate 2.5D images that facilitate extracting precise stoma contours. Among the six stoma models used, our algorithm exhibited errors within the range of 0 to 5.65 mm, with average errors below 2.55 mm, for four models. This level of accuracy is nearing our objective of maintaining errors less than 2 mm. Nevertheless, we encountered inaccuracies, stemming from the reconstructed 3D models and from failure to identify the stoma based solely on its topology dues to its complex nature and surrounding environment.

Our study was constrained by several limitations. First, it presumed stomas to be situated on a flat surface, which is not the case in actual clinical scenarios. Second, manual processing of the 3D scans was necessary, which involved cropping and leveling, potentially introducing errors. Lastly, our research involved a relatively limited range of stoma types. Future investigations should extend to include prolapsed stomas, stomas in close proximity to hernias, and stomas situated within body creases, as these variations present unique challenges in contouring. Our study serves as a foundation for further work in this direction, which we believe can significantly contribute to advancements in stoma care and management.

ACKNOWLEDGMENT

This material is based upon work supported by the National Science Foundation under Grant No. 2229218. We gratefully acknowledge the support of the University of Washington's Royalty Research Fund, which made this project possible. Our sincere thanks go to Nurse Practitioner Quyen Stevenson, whose medical expertise significantly enriched our understanding and guided the direction of our project.

REFERENCES

- [1] F. L. Monroy, R. Hussein, and A. Mamishev, "Accuracy of Smartphone Depth Cameras in Stoma Shape Extraction for Wafer Fitting," in 2022 Signal Processing: Algorithms, Architectures, Arrangements, and Applications (SPA), 2022: IEEE, pp. 40-45.
- [2] R. Hussein et al., "Remote Hub Lab-RHL: Broadly Accessible Technologies for Education and Telehealth," in International Conference on Remote Engineering and Virtual Instrumentation REV, 2023.
- [3] D. Anisuzzaman, C. Wang, B. Rostami, S. Gopalakrishnan, J. Niezgoda, and Z. Yu, "Image-based artificial intelligence in wound assessment: A systematic review," *Advances in Wound Care*, vol. 11, no. 12, pp. 687-709, 2022.
- [4] Y. Lucas, R. Niri, S. Treuillet, H. Douzi, and B. Castaneda, "Wound size imaging: ready for smart assessment and monitoring," *Advances in wound care*, vol. 10, no. 11, pp. 641-661, 2021.

- [5] R. Styliński, A. Alzubedi, and S. Rudzki, "Parastomal hernia-current knowledge and treatment," *Videosurgery and Other Miniinvasive Techniques*, vol. 13, no. 1, pp. 1-8, 2018.
- [6] S. Wang et al., "A new smart mobile system for chronic wound care management," *IEEE Access*, vol. 6, pp. 52355-52365, 2018.
- [7] T. W. K. Poon and M. R. Friesen, "Algorithms for Size and Color Detection of Smartphone Images of Chronic Wounds for Healthcare Applications," *IEEE Access*, vol. 3, pp. 1799-1808, 2015, doi: 10.1109/ACCESS.2015.2487859.
- [8] U. Pavlovčič and M. Jezeršek, "Handheld 3-dimensional wound measuring system," Skin Research & Technology, Article vol. 24, no. 2, pp. 326-333, 2018, doi: 10.1111/srt.12434.
- [9] V. Mamone, M. D. Fonzo, N. Esposito, M. Ferrari, and V. Ferrari, "Monitoring Wound Healing With Contactless Measurements and Augmented Reality," *IEEE Journal of Translational Engineering in Health and Medicine*, vol. 8, pp. 1-12, 2020, doi: 10.1109/JTEHM.2020.2983156.
- [10] D. Sánchez-Jiménez, F. F. Buchón-Moragues, B. Escutia-Muñoz, and R. Botella-Estrada, "SfM-3DULC: Reliability of a new 3D wound measurement procedure and its accuracy in projected area," *International wound journal*, vol. 19, no. 1, pp. 44-51, 2022, doi: 10.1111/iwj.13595.
- [11] E. Sirazitdinova and T. M. Deserno, "System design for 3D wound imaging using low-cost mobile devices," in *Medical Imaging 2017: Imaging Informatics for Healthcare, Research, and Applications*, 2017, vol. 10138: SPIE, pp. 258-264.
- [12] A. F. M. Hani, N. M. Eltegani, S. H. Hussein, A. Jamil, and P. Gill, "Assessment of Ulcer Wounds Size Using 3D Skin Surface Imaging." Berlin, Heidelberg: Berlin, Heidelberg: Springer Berlin Heidelberg, pp. 243-253
- [13] M. Mizoguchi, M. Kayaki, T. Yoshikawa, M. Asano, K. Onishi, and H. Noborio, "Selection and Evaluation of Color/Depth Camera for Imaging Surgical Stoma," in *Human-Computer Interaction. Interaction Techniques and Novel Applications*, Cham, M. Kurosu, Ed., 2021// 2021: Springer International Publishing, pp. 601-614.
- [14] D. Filko, R. Cupec, and E. K. Nyarko, "Wound measurement by RGB-D camera," *Machine Vision and Applications*, vol. 29, no. 4, pp. 633-654, 2018/05/01 2018, doi: 10.1007/s00138-018-0920-4.
- [15] A. Shah, C. B. Wollak, and J. B. M. C. Shah, "Wound Measurement Techniques: Comparing the Use of Ruler Method, 2D Imaging and 3D Scanner," *The journal of the American College of Clinical Wound Specialists*, vol. 5, no. 3, pp. 52-57, 2015, doi: 10.1016/j.jccw.2015.02.001.
- [16] A. Yee, F. Meng, S. Yi, and J. Harmon, "An Innovative App for the Management of Chronic Wound Treatment," in 2018 IEEE/ACM International Conference on Connected Health: Applications, Systems and Engineering Technologies (CHASE), 26-28 Sept. 2018 2018, pp. 3-4, doi: 10.1145/3278576.3281273.
- [17] L. B. Jørgensen, J. A. Sørensen, G. B. Jemec, and K. B. Yderstraede, "Methods to assess area and volume of wounds - a systematic review," (in eng), *International wound journal*, vol. 13, no. 4, pp. 540-553, 2016, doi: 10.1111/iwj.12472.
- [18] J. M. Juszczyk et al., "Wound 3D Geometrical Feature Estimation Using Poisson Reconstruction," *IEEE Access*, vol. 9, pp. 7894-7907, 2021, doi: 10.1109/ACCESS.2020.3035125.
- [19] D. F. Redaelli, S. G. Barsanti, E. Biffi, F. A. Storm, and G. Colombo, "Comparison of geometrical accuracy of active devices for 3D orthopaedic reconstructions," *The International Journal of Advanced Manufacturing Technology*, vol. 114, no. 1, pp. 319-342, 2021/05/01 2021, doi: 10.1007/s00170-021-06778-0.
- [20] S. Suzuki, "Topological structural analysis of digitized binary images by border following," *Computer vision, graphics, and image processing*, vol. 30, no. 1, pp. 32-46, 1985.